

PRECISION MEASUREMENT OF THE HIGGS BOSON MASS AND SEARCH FOR  
DILEPTON MASS RESONANCES IN  $H \rightarrow 4\ell$  DECAYS USING THE CMS DETECTOR AT  
THE LHC

By

DANIEL “JAKE” ROSENZWEIG

A DISSERTATION PRESENTED TO THE GRADUATE SCHOOL  
OF THE UNIVERSITY OF FLORIDA IN PARTIAL FULFILLMENT  
OF THE REQUIREMENTS FOR THE DEGREE OF  
DOCTORATE OF PHILOSOPHY

UNIVERSITY OF FLORIDA

2022

© 2022 Daniel “Jake” Rosenzweig

I dedicate this to Jacob Myhre.

## ACKNOWLEDGEMENTS

Without so many two-legged blessings along the way, I could never have made it to this point in my academic career. Thus, I give my unlimited thanks to the following people.

To my wife, Suzanne Rosenzweig, for showing me that dreams do come true. To my mother and father, Vicki and John, who always reassured me that I could achieve anything I put my mind to. Sleep peacefully, Mom. To my siblings, Alex, Ryan, Devin, Jace, and Claudia who frequently and gently reminded me that there was life outside of grad school.

To my mentor, Sheldon Friedman, and his wife, Rita Friedman (Rosenzweig), who chose to invest in my success at a young age To Sheldon's best friend, Dr. Bernard Khoury,

To my physics mentors, Professors Andrey Korytov and Guenkah Mitselmakher, for granting me the one-of-a-kind opportunity to work on the CMS Experiment at CERN. To Dr. Filippo Errico for his To Dr. Noah Steinberg To Darin Acosta, for spending hours of discussion on every t To the gentle gents who introduced me to the world of CMS, Brendan Regnery and Bhargav Joshi.

To my comrades for showing me what it takes to survive the core courses, Dr. Atool Divakarla, Dr. Brien O'Brendan, Dr. Daniel Guerrero, and Dr. Vladinar Martino.

To the grad students who tagged along in our "CMS Office Hours": Evan Koenig, Nik Menendez, Neha Rawal, John Rötter. And to the many students who let us practice our spiels: Sean Kent, Jeremiah Anglin, Cris Caballeros, Ari Gonzalez,

To my mentee, Matthew Dittrich, for

To my Polish roommates in Saint-Genis-Pouilly for showing me what home away from home feels like.

To the many moms who generously gave unconditional support during the darkest times and unconditional love during the brightest times: Silet Wiley, Margaret Sherrill, Dawn Hood, Cyndi Reilly-Rogers.

To my childhood best friends (in order of appearance): Jish, Willis, Shane, Zac, Duck, Marcus for their constant clever competition which has shaped me into the determined man I am today.

And finally to Existence itself for this unpredictable, unbelievable blip of an experience called life.

## TABLE OF CONTENTS

	<u>page</u>
ACKNOWLEDGEMENTS .....	4
LIST OF TABLES.....	6
LIST OF FIGURES.....	8
CHAPTER	
1    INTRODUCTION .....	10
2    THE CMS DETECTOR.....	11
2.1  The Silicon Tracker .....	14
2.1.1  The Pixel Detector.....	14
2.1.2  The Strip Detector .....	16
2.2  The Calorimeters .....	16
2.2.1  Electromagnetic Calorimeter.....	16
2.2.2  Hadron Calorimeter.....	19
2.3  The Solenoid and the Steel Return Yoke.....	21
2.4  The Muon System .....	23
2.4.1  Cathode Strip Chambers .....	24
2.4.2  Drift-Tube Chambers .....	29
2.4.3  Resistive Plate Chambers.....	32
2.4.4  Gas Electron Multipliers (GEM).....	32
3    SUMMARY .....	33

## LIST OF TABLES

Tables

page

## LIST OF FIGURES

<u>Figures</u>	<u>page</u>
2-1 Life-size poster of the CMS detector, taken during CERN Open Days 2019 in the SX5 warehouse where parts of CMS were assembled. ....	11
2-2 Points 1 through 8 along the LHC. Collisions occur at Points 1 (ATLAS), 2 (ALICE), 5 (CMS), and 8 (LHCb), whereas the remaining points are used for LHC beam maintenance and testing. ....	12
2-3 Cut out of the CMS detector showing its various subdetector components. ....	13
2-4 A transverse view of CMS showing the “filtration process” as different particles pass through different subdetectors. A positron (solid red line) curves due to the presence of the magnetic field and gets stopped in the ECAL, creating an EM shower. A photon (blue dashed line) does not get detected at all by the Silicon Tracker, since it has no electric charge. It continues through to the ECAL and makes a shower here, like the positron. Charged hadrons (solid green line) will show curved tracks from the Silicon Tracker, may leave some trace in the ECAL, but primarily get stopped by the HCAL creating hadronic showers. Neutral hadrons (dashed green line) do not interact with the tracker, and only undergo EM showers a little in the ECAL, but show most energy deposits in the HCAL. Muons (solid blue line) are detected by the Silicon Tracker and then mostly pass through the other subdetectors without interacting until they finally reach the Muon System. Using the Lorentz force law and knowing which direction the magnetic field is pointing, one can deduce the sign of the charge of the particle. Based on the radius of curvature from the trajectory, one can then calculate the momentum and energy of the particle. ....	15
2-5 (Left) A simulation of the silicon tracker, showing the 3 cylindrical layers of the pixel detector (pink), 4 layers of the TIB (green), and the 6 layers of the TOB (blue) of the strip detector. The endcap components are also shown. (Right) A picture of the real silicon tracker at the center of CMS. ....	16
2-6 A transverse view of the silicon pixel and strip detectors, explicitly labelling the different layers involved. ....	17
2-7 (Left) Cross sectional view of the electromagnetic calorimeter of CMS. (Right) One of the Dees which comprise the EE. Each square of $5 \times 5$ crystals constitutes a “supercrystal”. Figure taken from Ref.REFERENCE JINST.....	18
2-8 (Left) ECAL crystals made from PbWO <sub>4</sub> are grown in a lab. (Right) Although made mostly of metal, ECAL crystals are transparent and have a photomultiplier detector attached at the end.....	18
2-9 A cross-sectional quadrant of CMS showing the locations of the HCAL components: the barrel (HB), outer (HO), endcap (HE), and forward (HF) detectors. ....	21
2-10 A longitudinal cross section of CMS showing the values of the magnetic field over the volume of CMS and various field lines. The magnetic field reaches its maximum of 3.8 T in the center of the detector. ....	22

2-11 (Left) A simulated cut out view of the ME+ endcap, with the coordinate system of CMS in the top-left corner. (Right) The actual ME-2 disk of CMS is shown, revealing its ME-2/1 and ME-2/2 rings of CSCs. ....	24
2-12 Longitudinal cross section of CMS, showing the different pseudorapidity values ( $\eta$ ) and also the different subdetector regions. ....	25
2-13 Exploded view of the cross section of a CSC showing how the 7 panels come together to form the 6 gas gaps between the panels. ....	26
2-14 (Left) A CSC with its top layer exposed. You can see very thin gold-plated tungsten wires which actually span the entire width of the CSC. Thicker vertical strips run along the length. (Right) More detail showing the radial strips and the horizontal wires. Also shown is the 5 segments of a CSC. ....	27
2-15 A muon passes through one of the gaseous layers of the CSC, ionizing the gas mixture and inducing a charge on the anode wires and cathode strips. ....	28
2-16 (Left) Comparators are used to compare neighboring strip cluster charge to determine on which half-strip the peak charge resided. (Right) A muon passes through all six layers of a CSC inducing charge on various half-strips. ....	28
2-17 A drift-tube chamber with 3 superlayers (SLs) is sandwiching a honeycomb plate. Two SLs are indicated by the blue rectangles, whose cells (orange rectangle) have anode wires (red dots) oriented parallel to the beam pipe. The third SL is indicated by the green rectangle and is staggered orthogonally to the other two SLs. ....	30
2-18 A cross section of a DT cell showing the drift lines (light blue), isochrone lines (dark blue), dimensions of the cell, and locations of the anode wire and cathode strips. ....	31
2-19 A cross section of CMS showing the locations and numbering scheme of the drift tubes in the barrel. ....	31



## CHAPTER 1 INTRODUCTION

The universe, while overwhelmingly vast, is comprised of a curiously small number of elementary particles. These particles and their strong, weak, and electromagnetic interactions with each other are accurately described by the Standard Model (SM). A major shortcoming of the SM was its inability to predict the masses of these particles.

This dissertation presents a precision measurement of the Higgs boson mass and using LHC proton-proton collision data from Run 2 data set from

The SM was not able to predict the masses of these particles until 1964 when the Brout-Englert-Higgs mechanism suggested that It wasn't until 1964 that the Brout-Englert-Higgs mechanism gave a self-consistent way to : by breaking the electroweak gauge symmetry of the vacuum would give rise to non-zero masses of the weak gauge bosons. This would yield a secondary effect too: there should exist a fundamental scalar boson which is the quantum of the so-called “Higgs field”. On July 4th, 2012, this Higgs boson was discovered.

At first glance, the universe appears to be an overwhelmingly vast and complicated place. However upon closer inspection, it is comprised of only a few different kinds of fundamental particles. Particle physics has given rise to the Standard Model (SM) which mathematically describes these constituents and their interactions with each other.

The Standard Model (SM) is an impressively accurate mathematical theory which describes the fundamental particles of the universe and the rules for their possible interactions. Problematically though, the SM predicts that all particles are massless.

Get to the Higgs boson.

Why is it important? Knowing the mass of the Higgs boson

## CHAPTER 2

### THE CMS DETECTOR



Figure 2-1. Life-size poster of the CMS detector, taken during CERN Open Days 2019 in the SX5 warehouse where parts of CMS were assembled.

Weighing in at 14,000 tonnes, standing 5 stories tall (15 m), and reaching 29 m long, the Compact Muon Solenoid (CMS) experiment is one of two general-purpose particle detectors at the LHC (Fig. 2-1). CMS is situated approximately 100 m under the earth at the fifth collision point (Point 5) along the LHC (Fig. 2-2). In 2012, both CMS and its competing experiment, ATLAS, independently discovered the Higgs boson.

As discussed in Section (TODO: REF), the LHC collides bunches of protons every 25 ns to produce thousands of new particles which then travel away from the interaction point. CMS is built around the interaction point in a series of cylindrical subdetectors for nearly hermetic coverage so that most of the particles must travel through CMS. The detector sports a solenoid, after which CMS was named, which generates a 3.8 T uniform magnetic field that points longitudinally down the central axis of CMS. This strong magnetic field applies a Lorentz force on the outgoing charged particles, causing them to follow helical, momentum-dependent trajectories. These curved tracks are then better separated from one another which assists in particle identification. Neutral particles experience no Lorentz force and thus travel in straight lines.

The subdetectors measure the properties of the outgoing particles and carefully filter them out in a clever way (Fig. 2-3). Particles interact with the subdetectors, leaving so called “hits” where

they passed through. Hits are reconstructed into tracks. From the track curvature, deduce charge and momentum of the particles. Depending on which subdetector (or combination of subdetectors) was hit by the outgoing particles, the type of particle can be deduced. A few example particles

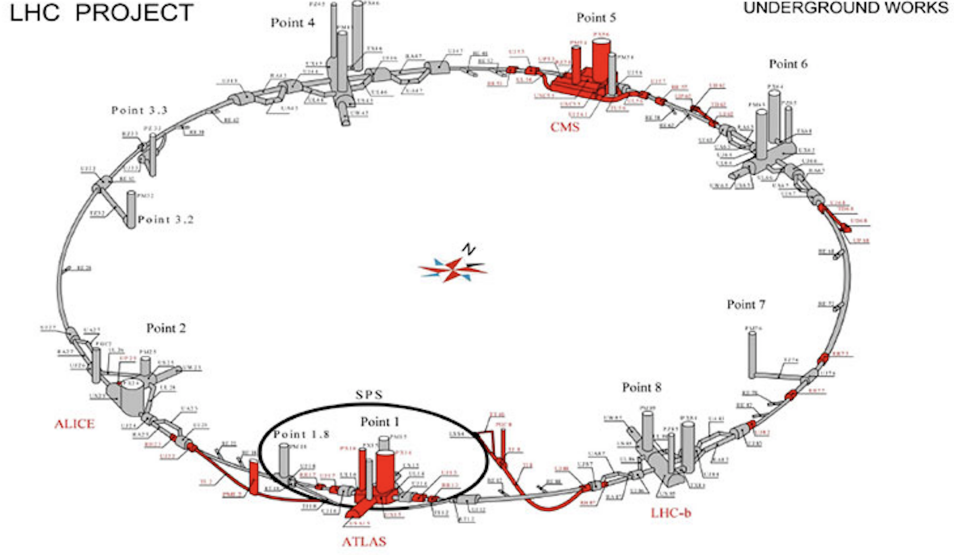


Figure 2-2. Points 1 through 8 along the LHC. Collisions occur at Points 1 (ATLAS), 2 (ALICE), 5 (CMS), and 8 (LHCb), whereas the remaining points are used for LHC beam maintenance and testing.

and their associated tracks are shown in Fig. 2-4.

Before discussing each subdetector in the following sections, it is useful to define the coordinate system used in CMS: a typical, right-handed, three-dimensional Cartesian coordinate system  $(x, y, z)$  is used, whose center  $(0, 0, 0)$  is placed at the nominal pp collision point within CMS. The  $x$ -axis points towards the center of the LHC, the  $y$ -axis points vertically upward, and the  $z$ -axis points westward towards the Jura mountains, tangential to the beam direction. Since CMS covers almost the entire spherical  $4\pi$  steradians around the interaction point, it is convenient to use spherical coordinates  $(r, \phi, \theta)$ , in which  $r$  measures the radial distance in the  $x$ - $y$  plane,  $\phi$  measures the azimuthal angle in the  $x$ - $y$  plane as measured from the  $x$ -axis, and  $\theta$  measures the polar angle as measured from the  $z$ -axis. When dealing with ultra-relativistic particles like those produced at the LHC, special relativistic effects like length contraction must be taken into account and so the coordinate  $\theta$  becomes frame-dependent. It is thus helpful to convert  $\theta$  to the Lorentz-invariant

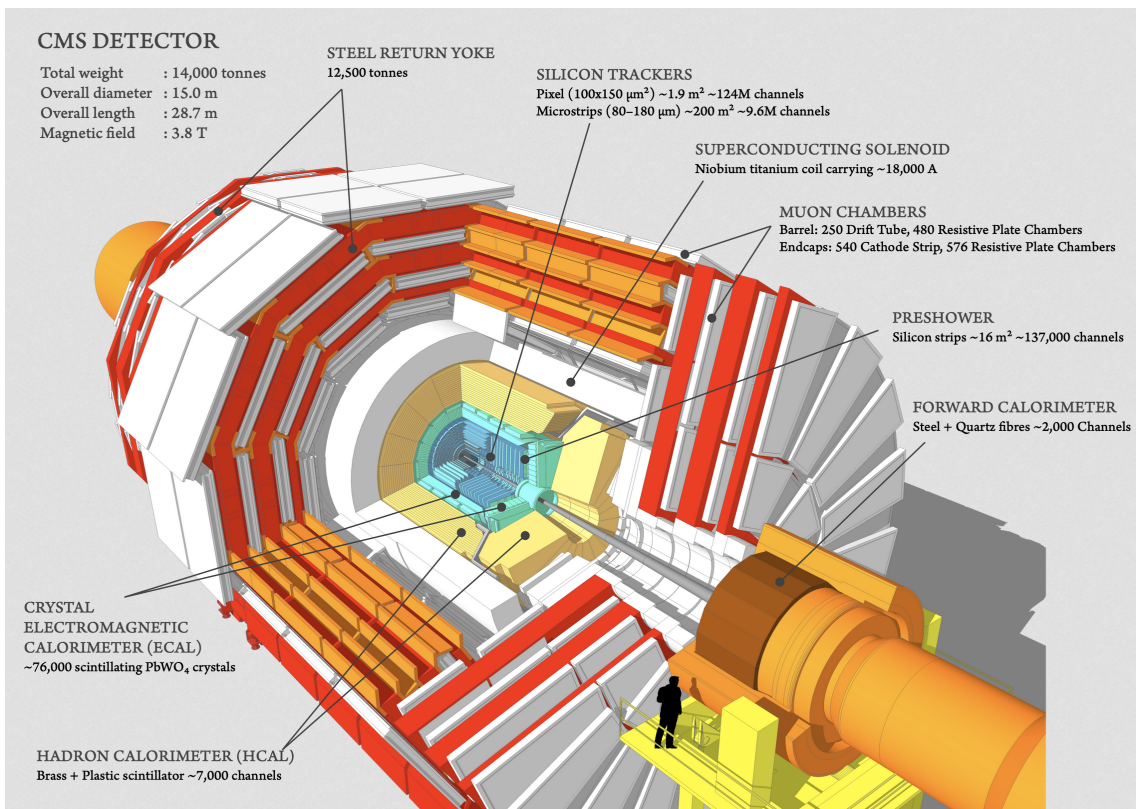


Figure 2-3. Cut out of the CMS detector showing its various subdetector components.

quantity called pseudorapidity ( $\eta$ ), which is defined as:

$$\eta = -\ln(\tan(\theta/2))$$

## 2.1 The Silicon Tracker

At the heart of CMS is one of the world’s largest silicon detectors: the silicon tracker. The main goal of the silicon tracker is not to capture outgoing particles but to very precisely measure the hits from the charged particles as they pass through it. The tracker also assists in vertex identification, differentiating between primary and secondary vertices, the latter of which often comes from B meson decays. When multiple pp collisions occur within the same BX (pile up), the tracker distinguishes between proton collisions with a resolution of about  $100 \mu\text{m}$  longitudinally and  $50 \mu\text{m}$  transverse to the beam pipe. This is crucial to resolve which outgoing particles came from which pp vertex.

The tracker consists of two types of pure silicon detectors: the pixel detector and the strip detector, each of which is described in detail below.

### 2.1.1 The Pixel Detector

The innermost part of the silicon tracker is the pixel detector, which is the closest subdetector to the interaction point. The pixel detector is composed of 66 million silicon “pixels”, as shown in Fig. 2-5 (Left, pink). A single pixel is  $100 \mu\text{m} \times 150 \mu\text{m}$  and, collectively, they cover a sensitive area of  $1.9 \text{ m}^2$ . Because it sits only 8 cm away from the beam pipe, the pixel detector receives the highest particle flux than any other subdetector: around 10 million particles per  $\text{cm}^2$  per second.

The pixel detector is made of three cylindrical layers and two endcaps that surround the beam pipe. In total, the pixel detector has around 6,000 connections (channels) per  $\text{cm}^2$ .

After the LHC Run 1 was completed, the accelerator received luminosity upgrades during the 2013-2014 long shutdown period. To handle these higher luminosities, the pixel detector was replaced by the CMS Phase-1 pixel detector during the LHC technical stop in 2016-2017. The upgrades outfitted the detector with four barrel layers and three endcap disks per side, which allowed

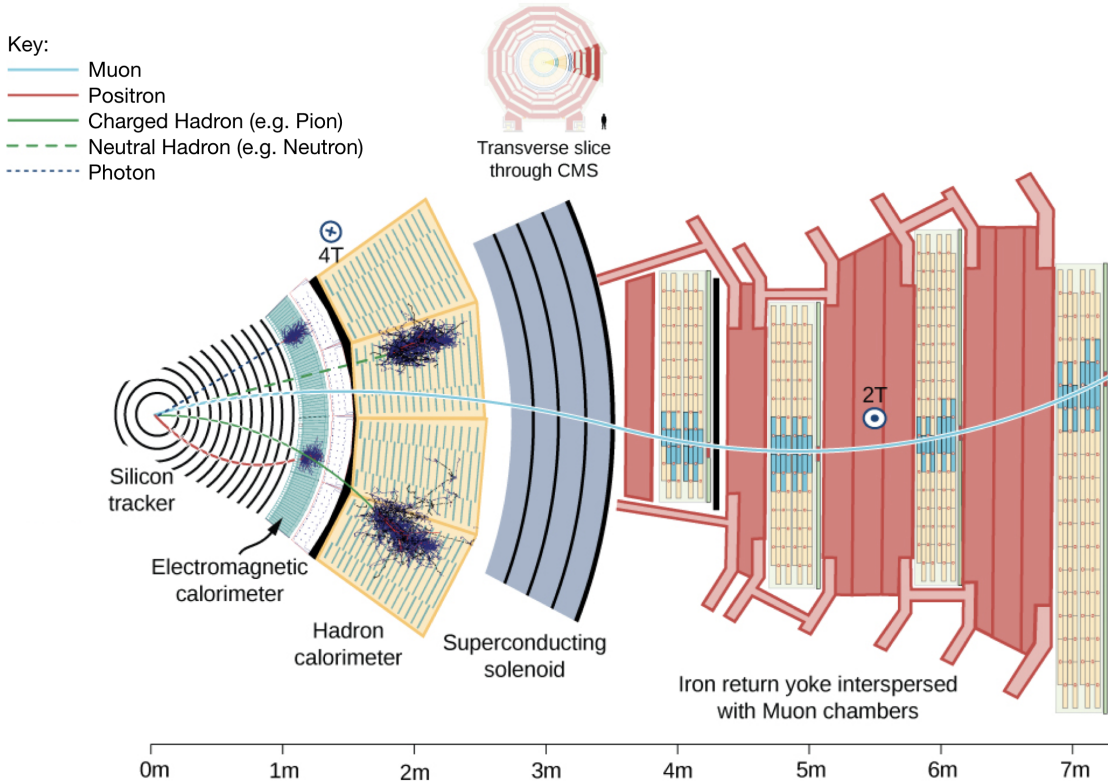


Figure 2-4. A transverse view of CMS showing the “filtration process” as different particles pass through different subdetectors. A positron (solid red line) curves due to the presence of the magnetic field and gets stopped in the ECAL, creating an EM shower. A photon (blue dashed line) does not get detected at all by the Silicon Tracker, since it has no electric charge. It continues through to the ECAL and makes a shower here, like the positron. Charged hadrons (solid green line) will show curved tracks from the Silicon Tracker, may leave some trace in the ECAL, but primarily get stopped by the HCAL creating hadronic showers. Neutral hadrons (dashed green line) do not interact with the tracker, and only undergo EM showers a little in the ECAL, but show most energy deposits in the HCAL. Muons (solid blue line) are detected by the Silicon Tracker and then mostly pass through the other subdetectors without interacting until they finally reach the Muon System. Using the Lorentz force law and knowing which direction the magnetic field is pointing, one can deduce the sign of the charge of the particle. Based on the radius of curvature from the trajectory, one can then calculate the momentum and energy of the particle.

for particle detection up to  $|\eta| < 2.5$ . The overall mass of the pixel detector decreased and granted the detector with better tracking capability.

### 2.1.2 The Strip Detector

The outer part of the silicon tracker is called the strip detector, which has 10 million detector strips spread across 10 cylindrical layers. The first 4 layers belong to the tracker inner barrel (TIB) and the remaining 6 layers belong to the tracker outer barrel (TOB), Fig. 2-5 (Left, green and blue, respectively). Both the TIB and TOB have two endcaps associated with them, the TID and TEC, respectively. Accounting for all of its components, the strip detector is sensitive to  $200 \text{ m}^2$ . Fig. 2-6 gives a clearly-labelled transverse illustration of the pixel and strip detectors.

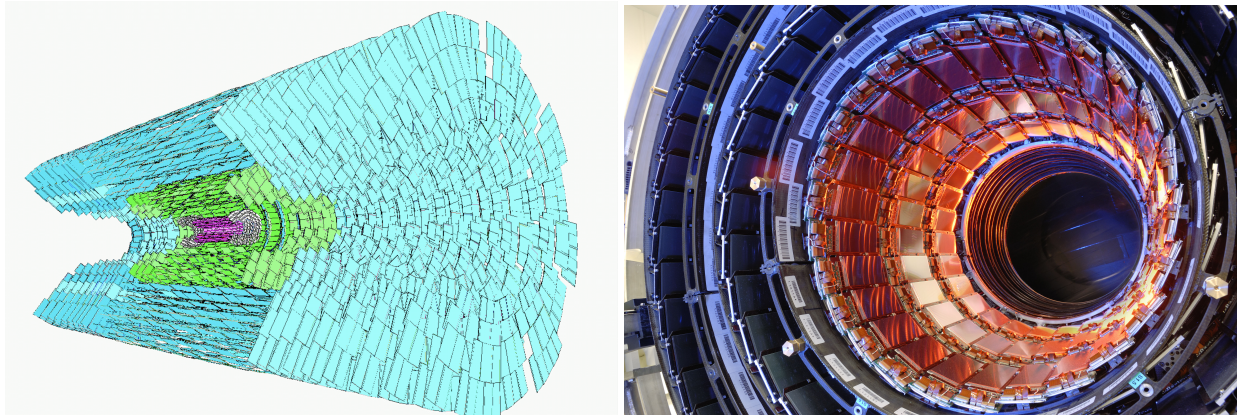


Figure 2-5. (Left) A simulation of the silicon tracker, showing the 3 cylindrical layers of the pixel detector (pink), 4 layers of the TIB (green), and the 6 layers of the TOB (blue) of the strip detector. The endcap components are also shown. (Right) A picture of the real silicon tracker at the center of CMS.

## 2.2 The Calorimeters

### 2.2.1 Electromagnetic Calorimeter

**Overview:** Particles that pass through the silicon tracker 2.1 encounter the electromagnetic calorimeter (ECAL). Those particles which interact electromagnetically but not strongly, mostly photons and electrons, are typically absorbed by the ECAL. The particle's energy is then transferred to the ECAL in the form of an electromagnetic (EM) shower. The size and shape of the EM shower provide information about the particle's energy and trajectory. Since the Higgs boson can decay into two photons, it was essential that the ECAL was able to detect this decay mode.

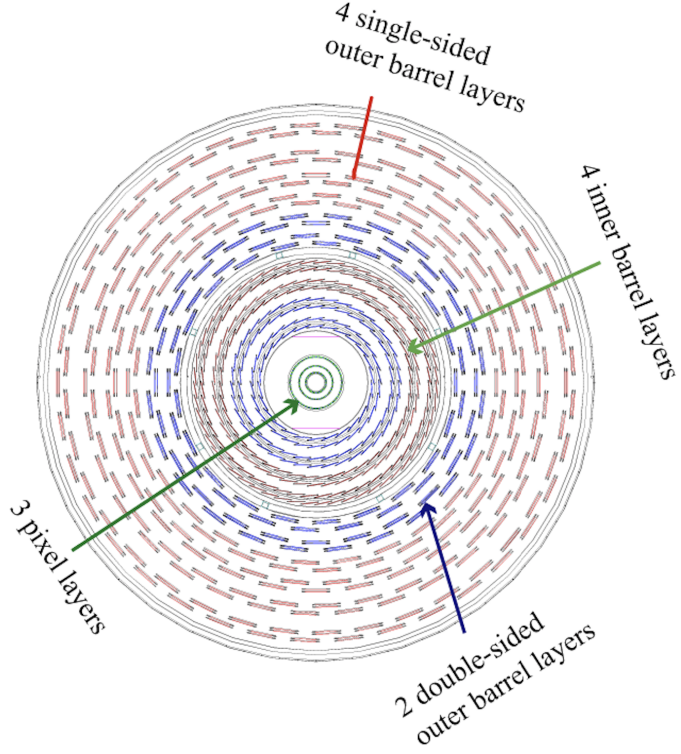


Figure 2-6. A transverse view of the silicon pixel and strip detectors, explicitly labelling the different layers involved.

**Design:** The ECAL is a hermetic, cylindrical, homogeneous sub-detector that consists of a barrel (EB), two endcaps (EE), and a preshower detector in front of each endcap (Figure 2-7, Left). The EB covers  $|\eta| < 1.479$  while the EE covers  $1.479 < |\eta| < 3.0$ . The entire subdetector is composed of transparent lead tungstate ( $\text{PbWO}_4$ ) crystals that point axially towards the center of CMS (the interaction point). The transparent crystals, one of which is shown in Fig. 2-8 (Left), have a high density ( $8.28 \text{ g/cm}^3$ ) which provides the ECAL with radiation resistance and a short radiation length ( $X_0 = 0.89 \text{ cm}$ ). Because so many crystals are used (61,200 crystals in the EB and 7,324 in the EE), the ECAL has excellent energy resolution and fine granularity. Each endcap is composed of two “Dee”s, one of which is shown in Figure 2-7 (Right). A single Dee carries 3,662 crystals. Crystals in the barrel are tapered, having front face dimensions  $2.2 \times 2.2 \text{ cm}^2$ , back face dimensions  $2.6 \times 2.6 \text{ cm}^2$ , and are 23.0 cm long ( $25.8 X_0$ ). Crystals in the endcaps are also tapered, with front face dimensions  $2.862 \times 2.862 \text{ cm}^2$ , back face dimensions  $3.0 \times 3.0 \text{ cm}^2$ , and are 22.0 cm long ( $24.7 X_0$ ). This gives a single crystal from the barrel a volume of approximately 132.5

$\text{cm}^3$  (mL), about the volume of a small cup of coffee, yet it weighs 1.5 Kg. (REF:PDG). REF:PDG Particle Data Group collaboration, S. Eidelman et al., *Review of particle physics*, *Phys. Lett. B* **592** (2004) 1

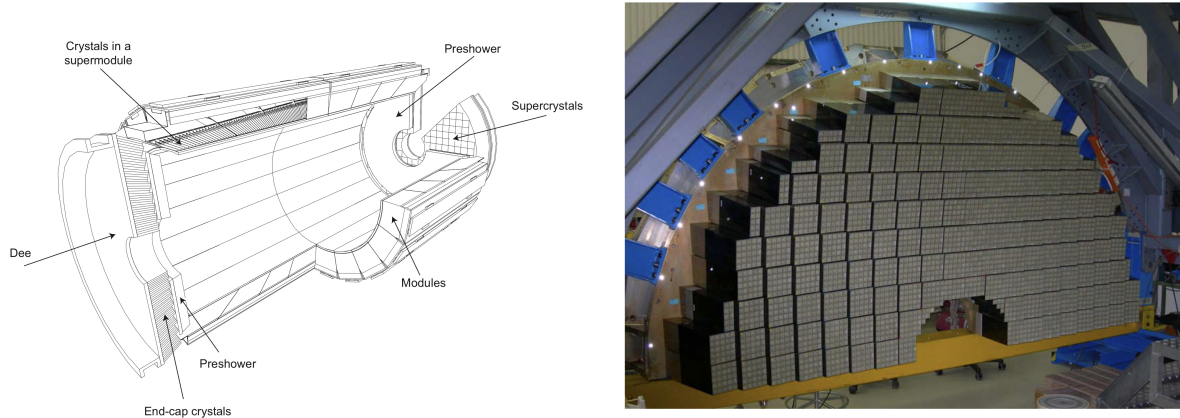


Figure 2-7. (Left) Cross sectional view of the electromagnetic calorimeter of CMS. (Right) One of the Dees which comprise the EE. Each square of  $5 \times 5$  crystals constitutes a “super-crystal”. Figure taken from Ref.REFERENCE JINST

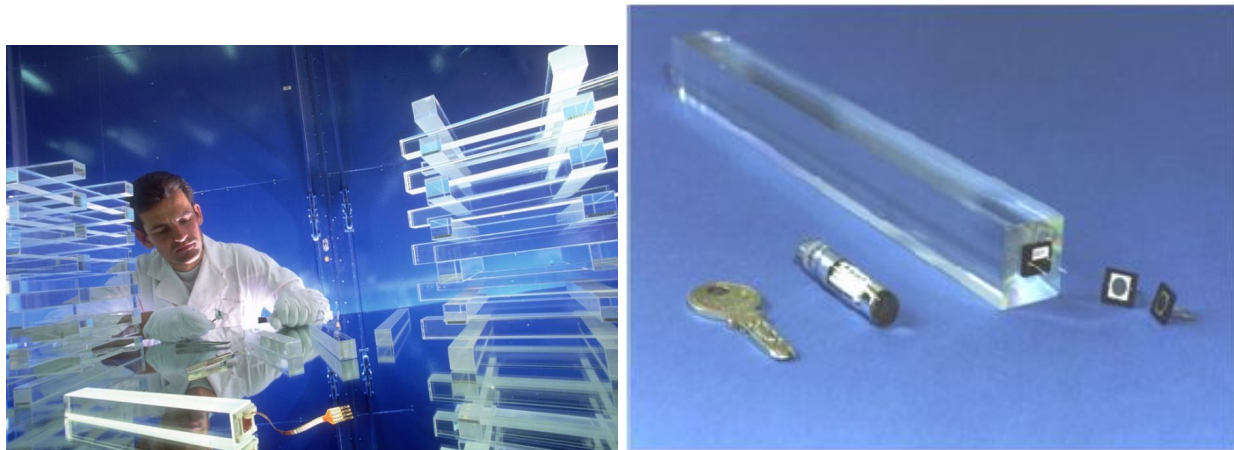


Figure 2-8. (Left) ECAL crystals made from PbWO<sub>4</sub> are grown in a lab. (Right) Although made mostly of metal, ECAL crystals are transparent and have a photomultiplier detector attached at the end.

**Physics:** When electrons or photons pass through the ECAL, they create an EM shower. Electrons radiate more photons as they accelerate around PbWO<sub>4</sub> nuclei, in a process called *bremssstrahlung*. Meanwhile, near the presence of a nucleus, high-energy photons pair produce into  $e^+e^-$ . This cycle of electron and photon production disperses the initial particle energy into a spray

of lower- and lower-energy particles; an EM shower (REFERENCE EM SHOWER FIG).

SHOW PICTURE OF EM SHOWER.

The ECAL crystals then scintillate (emits photons) in proportion to the amount of energy deposited by the interacting particle. The scintillator photons are detected by avalanche photodiodes on the back of each barrel crystal or by vacuum phototriodes in the endcap crystals (Fig. 2-8, Right). Conveniently after 1 bunch crossing (25 ns), Approximately 80% of the scintillated light is emitted.

An energy deposit in the ECAL could come from either an electron or a photon. In order to tell the difference, information from the silicon tracker is used. Charged particles, like electrons, will leave hits in the tracker and follow a curved path, whereas photons are electrically neutral and thus will not show any signs within the silicon tracker. So long as the tracker and ECAL communicate effectively with each other, then they help distinguish between electrons and photons. Charged hadrons interact only minimally with the ECAL, instead continuing on to the Hadron Calorimeter. Neutral hadrons can be detected by the ECAL preshower near the ECAL endcaps which helps distinguish a single photon from  $\pi^0$  mesons as they decay into two photons with a narrow opening angle, making it look as if the two photons are a single photon. The preshower detector allows CMS to distinguish between low-energy diphoton pairs and single high-energy photons.

NEED SMOOTH TRANSITION INTO HCAL. What about those hadrons? They got through the ECAL... To detect hadrons effectively, we need a Hadron Calorimeter.

### 2.2.2 Hadron Calorimeter

**Overview:** The particles that survive the ECAL, typically only muons and hadrons, then enter the hadron calorimeter (HCAL). Its primary purpose is to absorb the hadronic matter emerging from the interaction point and measure the corresponding jet energies. The absorbed jets cause the HCAL to scintillate photons which are then converted into electrical signals. These signals are used to deduce the original jet energies and any missing transverse energy ( $E_T^{\text{miss}}$ ) from the event.

**Design:** Dissimilar to the ECAL (subsec. 2.2.1) in material composition but similar in shape, the HCAL is a brass cylindrical scintillator. Although it has a barrel (HB) and two endcaps (HE),

it has two more detectors than the ECAL: the outer calorimeter (HO) and the forward calorimeter (HF). The HB spans the pseudorapidity range  $|\eta| < 1.3$ , the HE spans  $1.3 < |\eta| < 3$ , and the HF spans  $3 < |\eta| < 5.2$ , as shown in Figure 2-9. With a thickness of over 1m, the HB is sandwiched between the barrels of the ECAL and the solenoid (subsec. 2.3) at radial values  $r = 1.77$  m and  $r = 2.95$  m, respectively. Because the HB and HE are located within the solenoid’s strong magnetic field of 3.8 T, they both were both constructed out of a non-magnetic absorber called *C26000 cartridge brass*. This absorber has a density of 8.53 g/cm<sup>3</sup> and an interaction length ( $\lambda_I$ ) of 16.42 cm. The thickness of the HB increases as  $1/\sin\theta$  so that at  $|\eta| = 0(1.3)$  the absorber thickness is  $5.82(10.6)\ \lambda_I$ . The HB is composed of two half-barrels, where each half-barrel is built from 18 identical azimuthal wedges and each wedge spans 20°. Each wedge is divided into four  $\phi$  segments so that a single  $\phi$  segment spans  $\Delta\phi = 0.087$ .

Since the volume available to the HCAL is so limited, and in order to stop any particles that might traverse the entire HCAL and solenoid, the HO (the “tail catcher”) is situated outside the barrel of the solenoid. The HF is located 11.2 m from the interaction point.

All tiles within a single  $\phi$  segment are grouped together into a single tray unit. The scintillator is also segmented into 16  $\eta$  sectors, the first(last) of which is located at  $|\eta| = 0(1.3)$ . This way each tile covers  $(\Delta\eta, \Delta\phi) = (0.087, 0.087)$ . Each layer has 108 trays.

**Physics:** Since hadrons are the only particles to interact via the strong force, the HCAL is designed to have a high nuclear density. This ensures ample opportunity for hadrons to radiate gluons and convert with the Similar to the ECAL, the HCAL will scintillate in proportion to the amount of energy of the captured particle. The incoming hadrons will *hadronize* (i.e., produce a hadronic shower), generating jets of quarks and gluons which are bound in various ways forming protons, neutrons, pions, kaons, etc. Interestingly, the HCAL is made using over a million old, brass shell casings from the Russian Navy back from World War II.

About 34% of the particles produced from LHC pp collisions enter the HE region, so the HE was built to handle high rates (MHz).

The entire HCAL utilizes approximately 70,000 plastic scintillator tiles. The active material

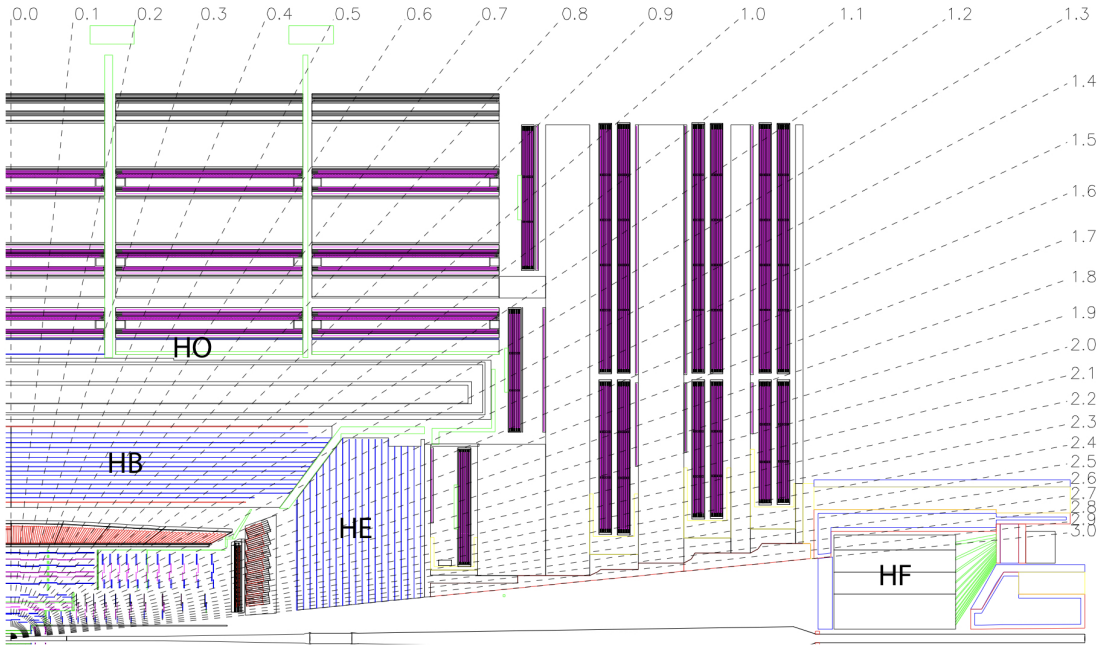


Figure 2-9. A cross-sectional quadrant of CMS showing the locations of the HCAL components: the barrel (HB), outer (HO), endcap (HE), and forward (HF) detectors.

in the HB is 3.7-mm-thick Kuraray SCSN81 plastic scintillator, selected for its radiation hardness and long-term stability. Hadron showers  $\rightarrow$  tiles scintillate  $\rightarrow$  scintillated photons are collected by 0.94-mm-diameter green double-cladded wavelength shifting (WLS) fibers (Kuraray Y-11), which carry the light to hybrid photodiodes (HPD).

### 2.3 The Solenoid and the Steel Return Yoke

The Compact Muon *Solenoid* sports one of the world's most energetic solenoids which is paramount to the success of CMS. Particles that exit the HCAL (subsec. 2.2.2) arrive at the cylindrical magnet which is 12.5 m in length, has a bore diameter of 6 m (6.3 m when cold), and generates a uniform 3.8 T magnetic field parallel to the beam line. To produce such a large and uniform magnetic field inside the approximately  $360 \text{ m}^3$  volume (Fig. 2-10), an 18,000 amp current travels through the 4-layer, superconducting, NbTi coils. This magnetic field is 100,000 times stronger than Earth field at the surface, storing a massive 2.6 GJ of energy—approximately the kinetic energy of an Airbus A320 in flight. The magnet has such a

large stored-energy-to-cold-mass ratio (11.6 KJ/Kg) that it experiences a physical deformation of 0.15% while energizing the field.

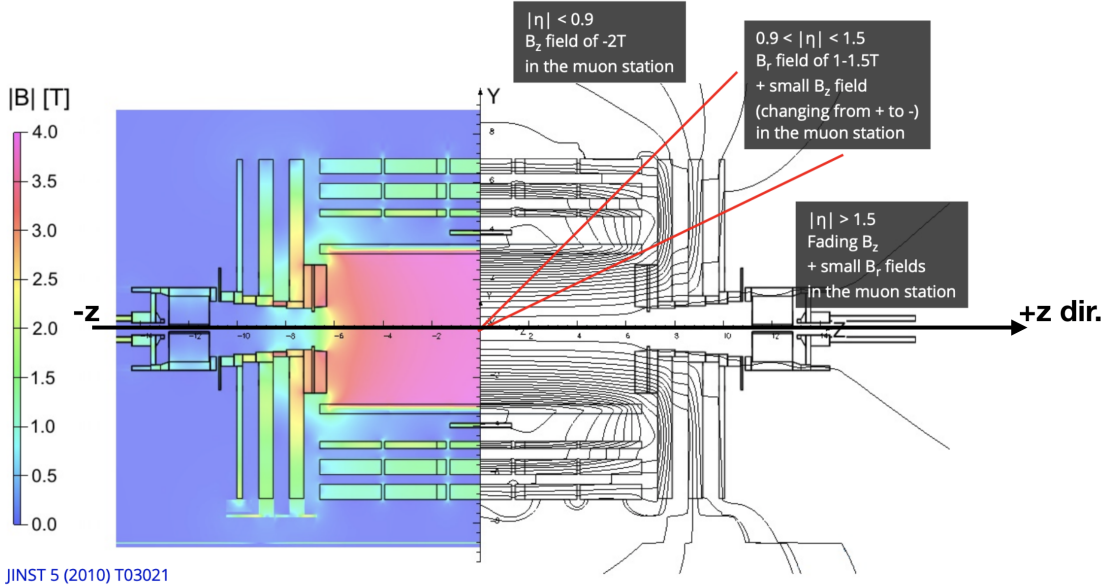


Figure 2-10. A longitudinal cross section of CMS showing the values of the magnetic field over the volume of CMS and various field lines. The magnetic field reaches its maximum of 3.8 T in the center of the detector.

As charged particles travel through any magnetic field, they experience a magnetic (Lorentz) force perpendicular to their direction of travel. The Lorentz force ( $\vec{F}_B$ ) exerted on a particle with charge  $q$  depends on the particle's velocity ( $\vec{v}$ ) and the strength of the magnetic field ( $\vec{B}$ ), given by

$$\vec{F}_B = q\vec{v} \times \vec{B}$$

Since the force is necessarily perpendicular to the velocity, the resulting trajectory is a helix. Projecting the helix on the  $x$ - $y$  plane (since the magnetic field points in the  $+z$  direction) allows the particle tracks to typically be separated from one another. Each track has a corresponding radius of curvature ( $R$ ) which relates to its transverse momentum ( $p_T$ ) through

$$p_T = qBR.$$

The relative change in  $p_T$  (i.e. the momentum resolution) is given by

$$\frac{\delta p_T}{p_T} \propto \frac{p_T}{BL^2}. \quad (2-1)$$

**Steel Return Yoke:** Most of the mass of CMS comes from the *steel return yoke* which helps to redirect the magnetic field back on itself. The yoke system constitutes 10,000 tonnes, which is 89% of the total mass of CMS. It is comprised of 5 wheels and 2 endcaps

## 2.4 The Muon System

Although it is the farthest system from the interaction point, the muon system is one of the most important within the Compact *Muon* Solenoid detector. Of the particles emerging from the interaction point, electrons and photons are absorbed by the ECAL (subsec. 2.2.1) and hadronic matter is absorbed by the HCAL (subsec. 2.2.2). This filtration process leaves only neutrinos and muons to enter the muon system, which is the outermost detector situated past the solenoid (sec. 2.3). As mentioned in , neutrinos are the only weakly-interacting, electrically-neutral SM particles which makes them incredibly difficult to detect directly. In fact, neutrinos interact with normal matter so little that a light-year (9.46 trillion Km) of lead would only stop half of the neutrinos moving through it. Thus, the detection of neutrinos produced from pp collisions is inferred via  $E_T^{\text{miss}}$  on a per-event basis. Muons, on the other hand, have a mass of 105.7 MeV (relatively heavy for a weakly-interacting, electrically-charged particle) and live a billion-billion times longer than a Higgs boson: the average lifetime of a muon is  $\tau_\mu = 2.2 \times 10^{-6}$  s. These properties are what determined the properties of the muon system within CMS to consist of its four main subdetectors, each of which is described in the following subsections:

1. CSC (cathode strip chambers, subsec. 2.4.1),
2. DT (drift tubes, subsec. 2.4.2),
3. RPC (resistive plate chambers, subsec. 2.4.3),
4. GEM (gas electron multiplier, subsec. 2.4.4).

### 2.4.1 Cathode Strip Chambers

**Overview:** A cathode strip chamber (CSC) is a multi-wire proportional chamber capable of precisely measuring the position of muons which enter and ionize the gas within. Spatial coordinates are obtained by the collection of electrical signals along the cathode strips ( $\phi$ ), anode wires ( $r$ ), and across multiple CSC layers ( $z$ ). CSCs are found exclusively on the two endcaps of CMS, with each endcap bearing 270 chambers (Fig 2-11). The chambers are arranged azimuthally around the beam pipe in four disks per endcap allowing for contiguous coverage in  $\phi$ . In total, the CSC system provides an effective detection area of about 5,000 m<sup>2</sup>, has a total gas volume that exceeds  $> 50$  m<sup>3</sup>, and contains over 400,000 read-out channels.

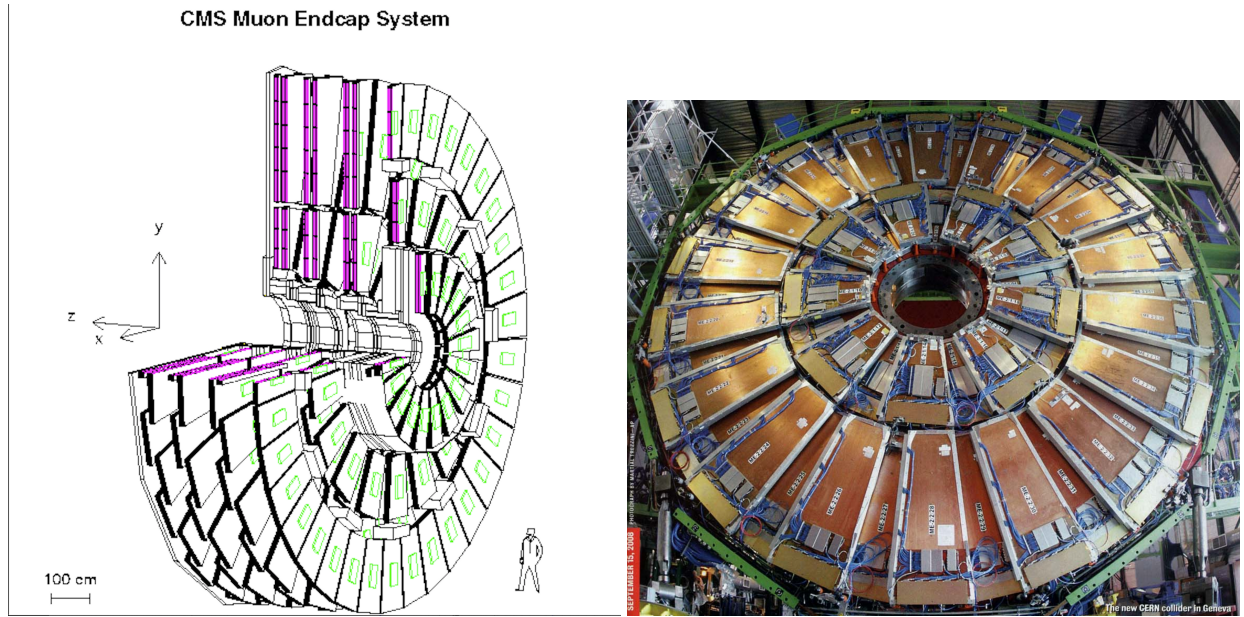


Figure 2-11. (Left) A simulated cut out view of the ME+ endcap, with the coordinate system of CMS in the top-left corner. (Right) The actual ME-2 disk of CMS is shown, revealing its ME-2/1 and ME-2/2 rings of CSCs.

**Design:** Each CSC is trapezoidal in shape with its narrow end pointed toward the beam pipe (Fig. 2-14, Left). The chambers are arranged in rings and each chamber subtends either 10° or 20° in  $\phi$ , as described in subsubsec. 2.4.1.1. The CSCs cover the pseudorapidity range of  $0.9 < |\eta| < 2.4$  (Fig. 2-12). A single CSC is composed of six layers (or *gas gaps*), each of which is filled with a carefully prepared gaseous mixture<sup>1</sup> of Ar:CO<sub>2</sub>:CF<sub>4</sub> (Fig. 2-13). The gas mixture flows from one

<sup>1</sup>The gas mixture ratio of Ar:CO<sub>2</sub>:CF<sub>4</sub> was chosen to be 5:4:1 to maximize the lifetime of the CSCs as they endure

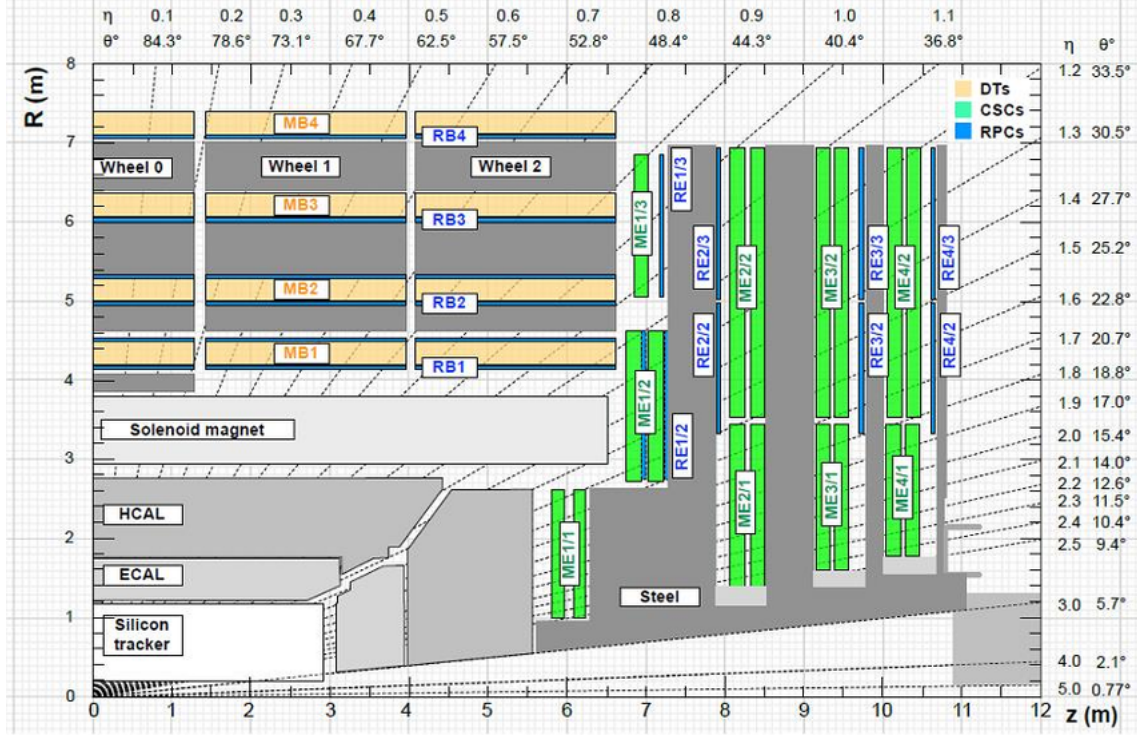


Figure 2-12. Longitudinal cross section of CMS, showing the different pseudorapidity values ( $\eta$ ) and also the different subdetector regions.

layer to the next in a zigzag manner and has a flow rate of ????. Within every layer, the gas mixture surrounds approximately 80 copper strips, each of which spans radially away from the interaction point. A single strip is about 8.4 mm wide at the narrower end of the CSC, about 16 mm at the wider end, and is separated from its neighboring strip by about 0.5 mm. Per layer, the inner gas also surrounds over 1,000 gold-plated tungsten wires, which are oriented azimuthally (so approximately orthogonal to the strips). Each wire is approximately 50  $\mu\text{m}$  in diameter and separated from its neighboring wire by about 3.2 mm. A collection of 16 consecutive wires forms a *wire group*, which is about 5 cm wide and creates a single anode read-out channel. A single wire plane has five independently controlled HV segments (Fig. 2-14, Right). The largest CSCs are 3.4 m long as measured along a strip and 1.5 m wide as measured along a wire.

**Physics:** As a muon passes through a CSC layer, it has the opportunity to interact with and ionize an Ar atom in the gas mixture. The wires are under high voltage (3,600 V) which radiation damage through years of use. The CO<sub>2</sub> is used as a non-flammable quencher to reach even larger electron multiplicities, while the CF<sub>4</sub> helps prevent polymerization along (aging of) the wires.

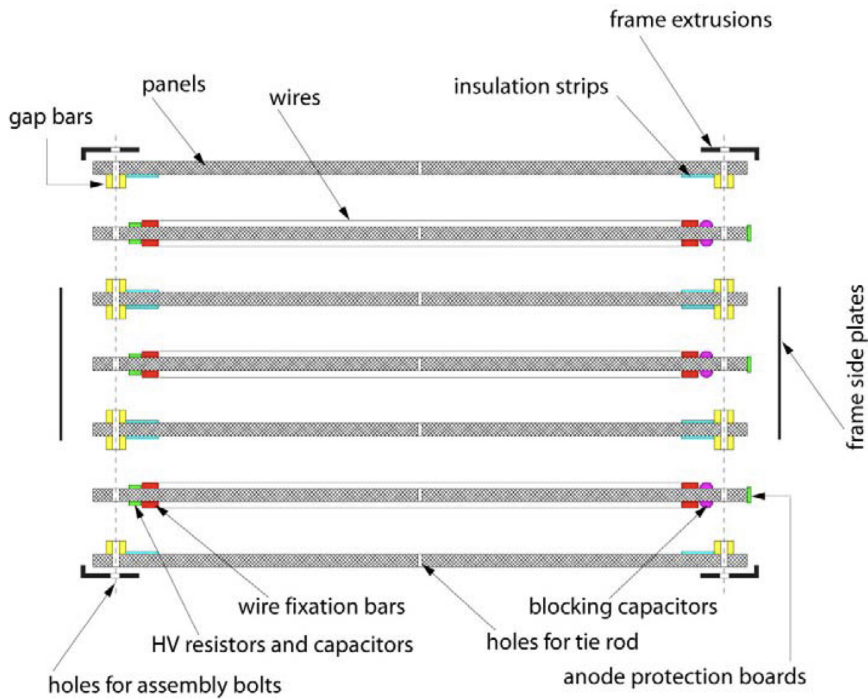


Figure 2-13. Exploded view of the cross section of a CSC showing how the 7 panels come together to form the 6 gas gaps between the panels.

causes the ionized electron to accelerate towards the positively-charged strips. The accelerating electron collides with and ionizes Ar atoms along its path toward the strip. This liberates even more electrons, thus forming an *electron avalanche* (Fig. 2-15). The total number of ionized electrons per initial electron is referred to as the *multiplicity* (or *gas gain*), which can reach as high as 100,000.

The electron avalanche is collected by a cathode strip and becomes an electrical signal. This signal is processed by the cathode front-end boards (CFEBs). The  $\text{Ar}^+$  ions similarly distribute a charge signal onto the negative wires. The cluster of charge that arrives at a strip is more widely spread than the charge which arrives along a wire. Therefore, comparator logic is implemented on the strips to narrow down the precision to the order of  $100 \mu\text{m}$  by using half-strip information (Fig. 2-16).

The muon passes through the next 5 layers of the CSC, further ionizing the gas mixture and generating electrical signals along the wires and strips. A signal on a wire provides an  $r$ -coordinate, on a strip provides a  $\phi$ -coordinate, and through the other layers provides a  $z$ -coordinate. Taken

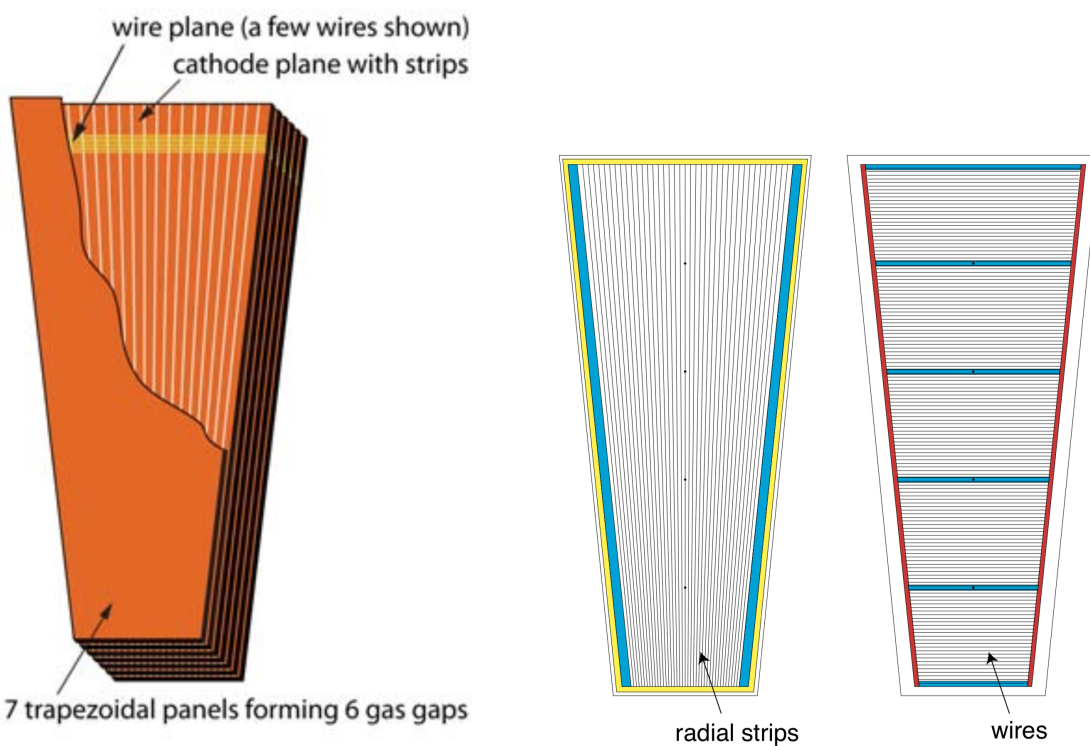


Figure 2-14. (Left) A CSC with its top layer exposed. You can see very thin gold-plated tungsten wires which actually span the entire width of the CSC. Thicker vertical strips run along the length. (Right) More detail showing the radial strips and the horizontal wires. Also shown is the 5 segments of a CSC.

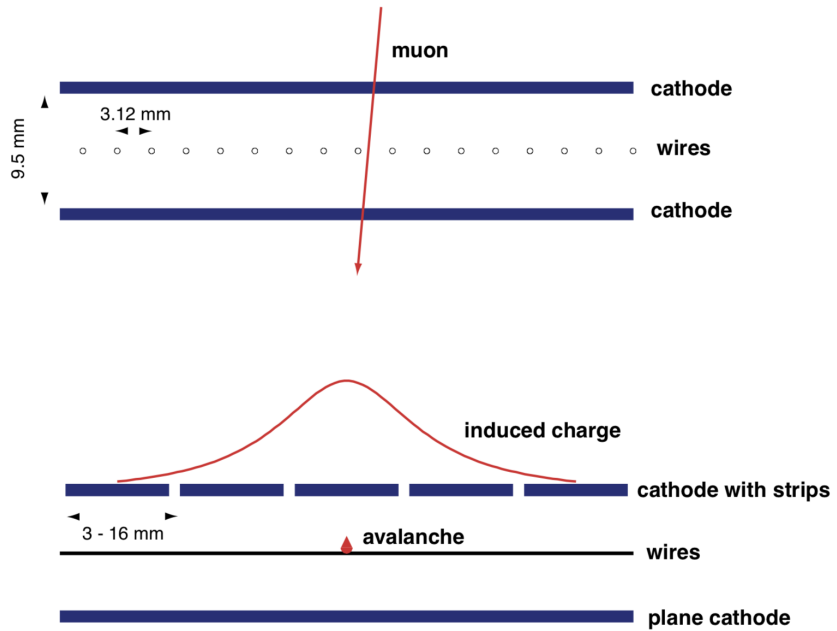


Figure 2-15. A muon passes through one of the gaseous layers of the CSC, ionizing the gas mixture and inducing a charge on the anode wires and cathode strips.

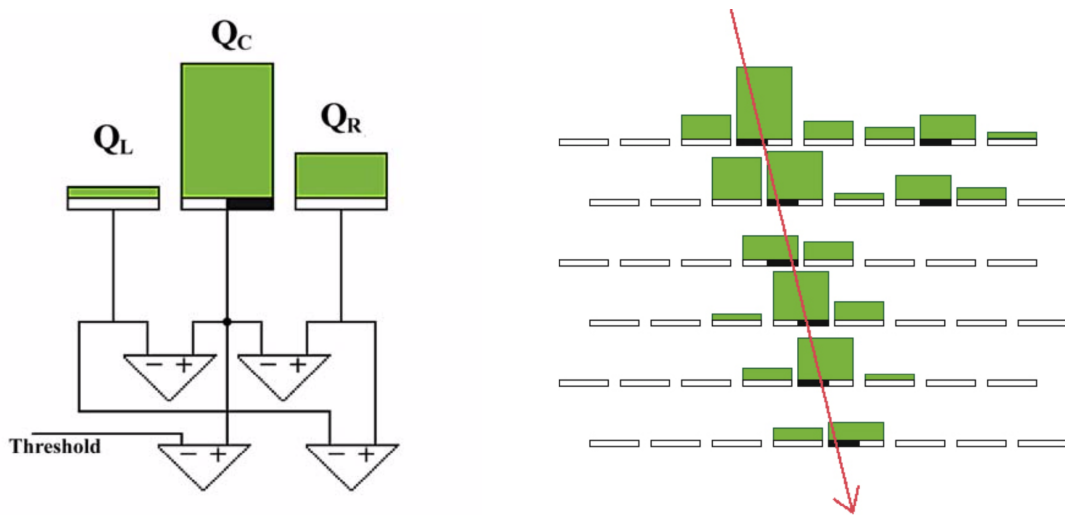


Figure 2-16. (Left) Comparators are used to compare neighboring strip cluster charge to determine on which half-strip the peak charge resided. (Right) A muon passes through all six layers of a CSC inducing charge on various half-strips.

together, this information helps to reconstruct the three-dimensional trajectory of the muon.

The number of hits recorded by the CSC will determine if an event was significant enough to be worth saving. If so, then its precise positions on the wires and strips will be read out by the Data Acquisition (DAQ) system and be stored for further data analysis. When a CSC is taking live data it can resolve approximately 2 mm in  $r\text{-}\phi$ , whereas during offline analysis the resolution improves by a factor of more than 20: the ME1/1 and ME1/2 chambers can resolve distances as small as 75  $\mu\text{m}$  in  $r\text{-}\phi$ , while the other chambers can resolve 150  $\mu\text{m}$ . It is worth noting that a CSC can accommodate up to 1 KHz/cm<sup>2</sup>.

Gas gap is 9.5 mm.

#### 2.4.1.1 CSC Numbering Scheme

The two endcaps are labelled as “ME+” and “ME-”, depending on whether they are situated in the  $+z$  direction or  $-z$ . Both endcaps are structurally symmetric, so it is sufficient to discuss only one in detail. The ME+ endcap has four disks: ME+1 is the first disk and the one closest to the interaction point, while ME+4 is the fourth and the farthest away. Within each disk, there are either two or three “rings” of CSCs, as shown in Fig. 2-12 (green). These rings are labelled as ME+ $D/R$ , where  $D$  indicates the disk number and  $R$  indicates the ring number. For example, ME+2/1 refers to the second disk and the first ring (the ring closest to the beam pipe). All rings contain 36 CSCs, except for ME $\pm X/1$ , for  $X = 2, 3, 4$ , which contain only 18 CSCs. Finally, the CSCs are given one final number to label them on the ring: the CSC that sits along the positive  $x$ -axis in the coordinate system of CMS is given the number “01”, e.g. ME+4/2/01. The CSCs are then numbered incrementally following the positive azimuthal direction.

#### 2.4.2 Drift-Tube Chambers

**Overview:** Functionally similar to but structurally different from a CSC (subsec. 2.4.1), a DT is a collection of gaseous detector cells (Fig. 2-17). A single DT cell has an anode wire and two cathode strips and operates on the same principle as a CSC, providing timing and position measurements of muons (Fig. 2-18). While CSCs are found only on the endcaps of CMS, drift-tube chambers (DTs) are placed exclusively along the barrel (Fig. 2-19). The DT system is

therefore composed of concentric cylindrical stations, with the central axis parallel to the beam pipe. Altogether, there are 250 DTs built inside of, between, and outside of the iron yoke.

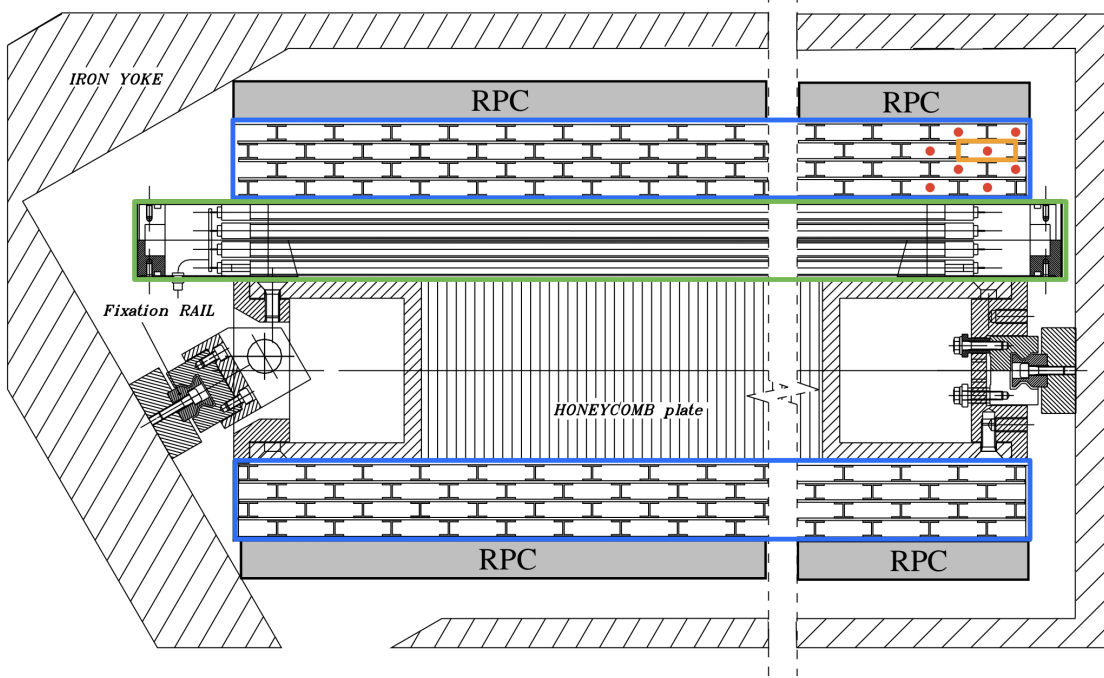


Figure 2-17. A drift-tube chamber with 3 superlayers (SLs) is sandwiching a honeycomb plate. Two SLs are indicated by the blue rectangles, whose cells (orange rectangle) have anode wires (red dots) oriented parallel to the beam pipe. The third SL is indicated by the green rectangle and is staggered orthogonally to the other two SLs.

**Design:** The first three stations contain 60 DTs each, while the station farthest from the beam pipe contains 70 DTs. The DTs are distributed among 5 wheels, 4 stations, and 12 sectors within the muon barrel (MB) system which uses the following numbering scheme: MB/W/A/S, where *W* is the wheel number (-2 to 2), *A* is the station number (1 to 4), and *S* is the sector number (1 to 12). This accounts for only  $5 \times 4 \times 12 = 240$  chambers, so the remaining 10 DTs are found in station 4, sectors 4 and 10, in each wheel (Fig. 2-19).

Each tube cross section is  $13 \times 42 \text{ mm}^2$ , within which a single anode wire is made of gold-plated stainless-steel that has a diameter of  $50 \mu\text{m}$ . Different voltages are applied to the anode wires (+3600 V), electrode strips (+1800 V), and cathode strips (-1200 V). The gas mixture within a DT is similar to that of a CSC, containing approximately 85% Ar + 15% CO<sub>2</sub>.

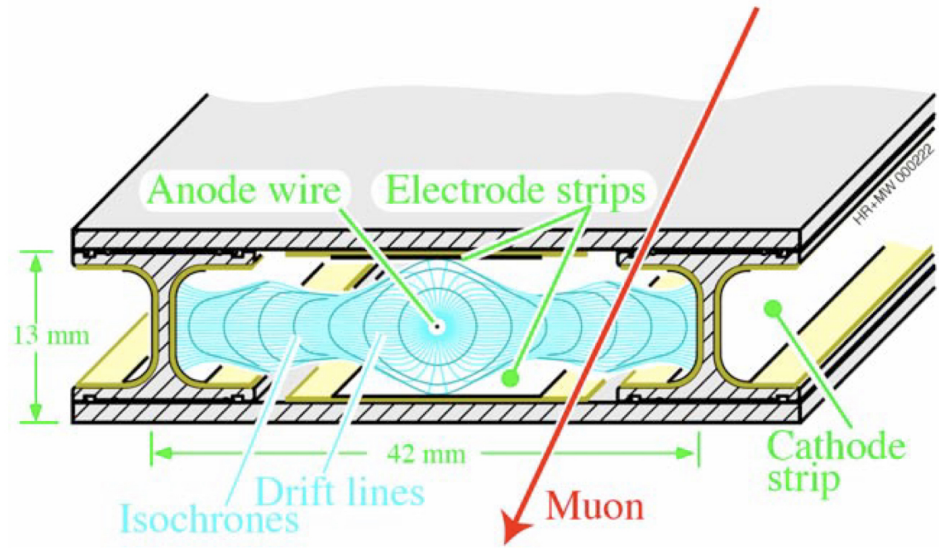


Figure 2-18. A cross section of a DT cell showing the drift lines (light blue), isochrone lines (dark blue), dimensions of the cell, and locations of the anode wire and cathode strips.

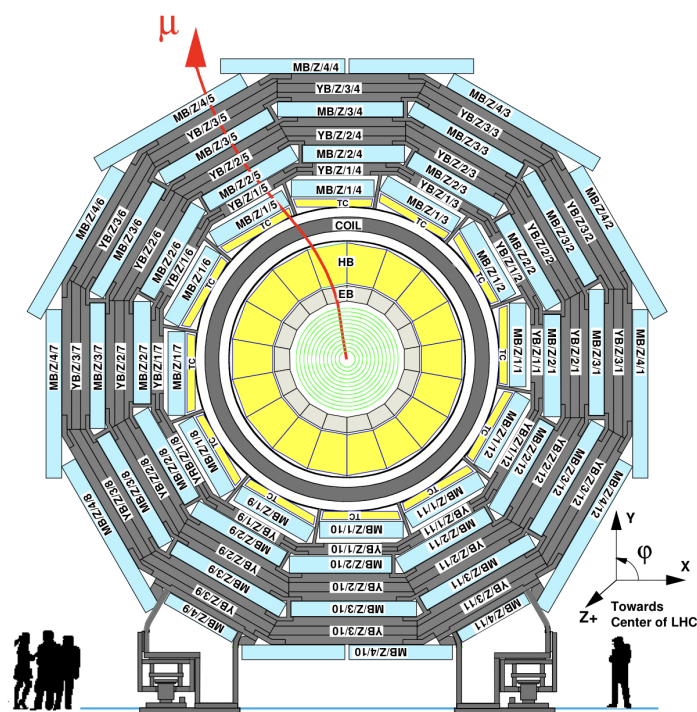


Figure 2-19. A cross section of CMS showing the locations and numbering scheme of the drift tubes in the barrel.

**Physics:** DTs are a good choice for the barrel because of the low rate and low strength of magnetic field. Uniform drift field of 1.5 KV/cm. A high  $p_T$  muon track will cross all 4 DT stations within the pseudorapidity range of  $|\eta| < 0.8$ . The reconstruction efficiency of such a track is better than 95%.

A single SL has a time resolution of only a few nanoseconds which provides excellent bunch crossing identification. To assist in determining muon  $p_T$  and timing, the DT system delivers the following muon track segment information to the L1 trigger: the position of the center of gravity (to a precision of 1.5 mm) and the corresponding angle (to a precision of 20 mrad), w.r.t. the SL reference frame. The total resolution of a DT in  $r-\phi$  is about 100  $\mu\text{m}$  which is comparable to the deviation caused by multiple scattering, for a muon with  $p_T \leq 200 \text{ GeV}$ .

The gas gain is comparable to that of a CSC (about 100,000).

The maximum drift distance in a DT is 21 mm, as can be seen in Fig. 2-18, which corresponds to a drift time of 380 ns. This value

### 2.4.3 Resistive Plate Chambers

**Overview:** Even though CSCs 2.4.1 and DTs 2.4.2 cover the entire pseudorapidity range of  $0 < |\eta| < 2.4$ , redundancy is important. Therefore, resistive plate chambers (RPCs) are placed in both the endcaps and barrel to provide excellent timing and spatial resolution, comparable to that of scintillators. An RPC is a gaseous parallel-plate detector

RPC has better time resolution than the 25 ns between two contiguous pp bunch crossings.

**Design:**

**Physics:**

### 2.4.4 Gas Electron Multipliers (GEM)

**Overview:**

**Design:**

**Physics:**

Located in the forward region. Filled with Ar/CO<sub>2</sub> gas mixture. The first GEMs At the time of this dissertation writing,

## CHAPTER 3 SUMMARY

words.